INTEGRAL

Science Operations Centre

Announcement of Opportunity for Observing Proposals (AO-8)

IBIS Observer's Manual

INT/OAG/10-0329/Dc

Issue 1.1

30 August 2010

Prepared by G. Bélanger

This page was intentionally left blank

Based upon inputs from:

P. Ubertini, IBIS Co-P.I., IASF-INAF, Rome
F. Lebrun, IBIS Co-P.I., CEA, Saclay
A. Bazzano, IASF-INAF, Rome
L. Natalucci, IASF-INAF, Rome
J. Lockley, University of Southampton
L. Foschini, IASF-INAF, Bologna
L. Bassani, IASF-INAF, Bologna
V. Bianchin, IASF-INAF, Bologna
D. Götz, CEA, Saclay
P. Barr†, ESA-ESTEC, Noordwijk
E. Kuulkers, ESA-ESAC, Madrid

Table of Contents

This page was intentionally left blank

1 Introduction

IBIS (**I**mager on **B**oard the **I**NTEGRAL **S**atellite) is one of the two prime instruments of the INTEGRAL scientific payload. This γ-ray telescope working in the energy range from ~15 keV to several MeV, observes various celestial objects from galactic X-ray binaries and cataclysmic variables, to active galactic nuclei and galaxy clusters. It has powerful diagnostic capabilities: fine imaging with localization of weak sources to within a few arcminutes, and good spectral sensitivity and resolution in the continuum and emission lines; these are overviewed in Table 1.

Table 1. IBIS technical specifications

Operating energy range	15 keV - 10 MeV
Continuum sensitivity[1] (ph cm^{-2} s^{-1} keV^{-1})	2.85×10^{-6} @ 100 keV 1.6×10^{-6} @ 1 MeV
Line sensitivity[2] (ph cm^{-2} s^{-1})	1.9×10^{-5} @ 100 keV 3.8×10^{-4} @ 1 MeV
Energy resolution (FWHM)	8% @ 100 keV 10% @ 1 MeV
Angular resolution (FWHM)	12'
Point source location accuracy (90% error radius)	1' for SNR = 30 (ISGRI) 3' for SNR = 10 (ISGRI) 5–10' for SNR = 10 (PICsIT)
Timing accuracy	61 μs - 1 hr
Field of view	8.33° × 8.00° (fully coded) 29.11° × 29.42° (zero response)

[1] Based on in-flight measurements; 3σ detection in10^5s, ΔE=E/2

[2] For a 3σ detection in 10^6 s

Imaging is performed using a coded mask. There are two detectors operating simultaneously; the **I**ntegral **S**oft **G**amma-**R**ay **I**mager, ISGRI, a semi-conductor array optimised at lower energies (15 keV – 1 MeV), and the **PI**xellated **C**ea**s**ium **I**odide (**CsI**) **T**elescope, PICsIT, a crystal scintillator for higher energies (175 keV – 10 MeV).

Figure 1 shows the total effective area of the two detectors as a function of energy, where absorption by parts of the instrument above the detector plane is taken into account (more details in §3.1.

In the following sections we provide detailed descriptions of the components that make up the IBIS telescope (§2), of how the instrument works (§3), and of its overall performance (§4). Section 5 is intended to provide help to prospective observers with a number of practical examples calculating observing times and expected detection significances.

More details on all aspects of the telescope can be found in the A&A special INTEGRAL issue (2003, Vol. 411, L131-L229). More specifically, for descriptions relating to the IBIS data analysis see Goldwurm et al. (2003, A&A 411, L223).

The validation reports by the ISDC of the **O**ff-line **S**cientific **A**nalysis (OSA) software, as well as descriptions of the data analysis modules and pipeline can be found in the *IBIS Analysis User Manual* from the ISDC web site: http://www.isdc.unige.ch/integral/download/osa_doc.

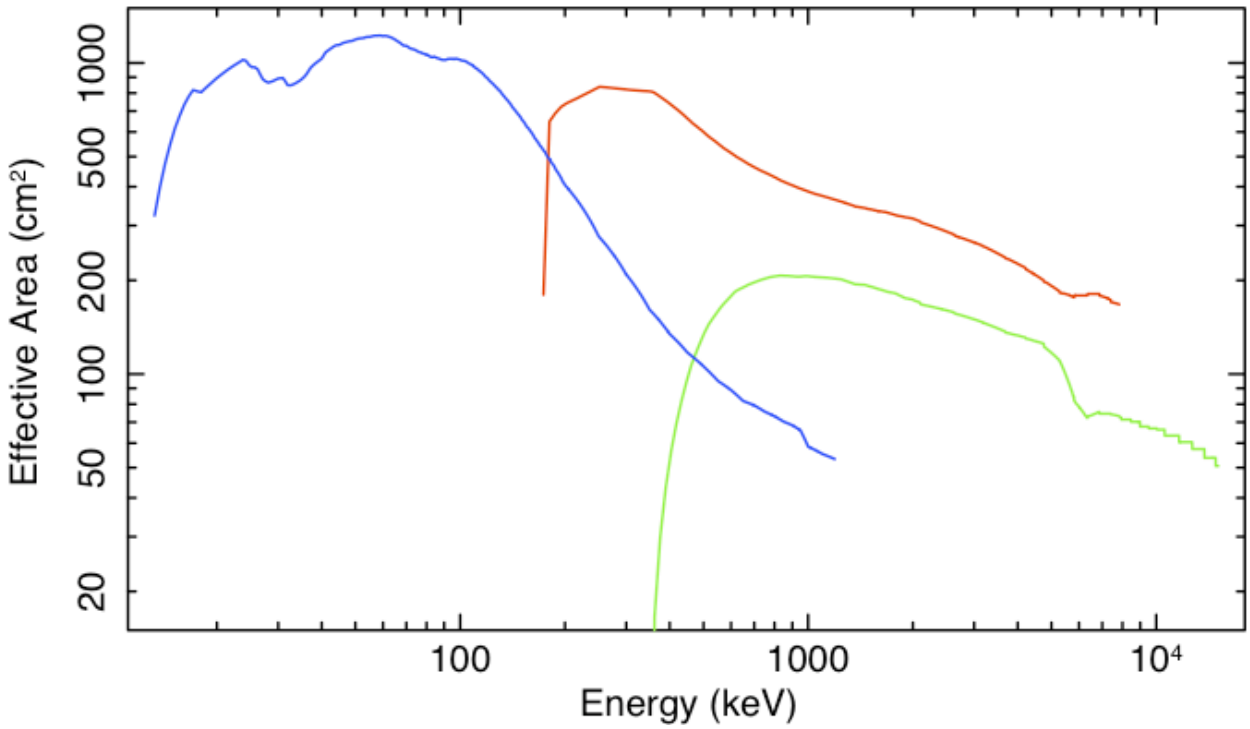

Figure 1: Ancillary response function: ISGRI (blue) and PICsIT (single: red, multiple: green).

2 Description of the instrument

2.1 The telescope

IBIS is a γ-ray imager operating in the energy range from 15 keV to 10 MeV. This range is covered by two simultaneously operating detectors located behind a Tungsten mask that provides the encoding by modulating the flux from astrophysical sources.

The coded mask is optimised for high angular resolution. As diffraction is negligible at γ-ray wavelengths, the angular resolution of a coded-mask telescope is defined by the ratio of the mask element size (11.2 mm) and the distance between the mask and the detection plane (3.2 m).

The detector is composed of two pixellated detecting layers: ISGRI (Lebrun et al., 2003, A&A, 411, L141) and PICsIT (Labanti et al., 2003, A&A, 411, L149). The first is made of Cadmium-Telluride (CdTe) solid-state detectors, and the second of Cesium-Iodide (CsI) scintillator crystals. This configuration ensures a good broad continuum and line sensitivity over a wide spectral range, and allows the paths of photons to be tracked in three dimensions, if the event triggers both ISGRI and PICsIT within 1.9 μs. The application of Compton reconstruction algorithms to these types of events (above a few hundred keV) allows, in principle, an increase in Signal-to-Noise Ratio (SNR) by rejecting events that are unlikely to correspond to source photons.

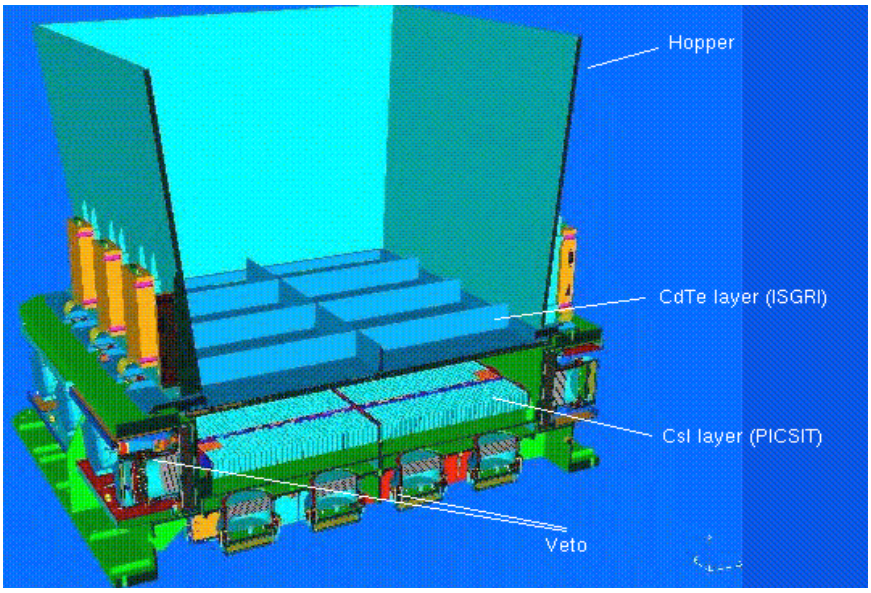

Figure 2. Cutaway drawing of the IBIS detector assembly together with the lower part of the collimator (''Hopper''). The coded mask (not shown) is located 3.2 m above the ISGRI detector

The detector aperture is restricted, in the hard X-ray part of the spectrum, by passive shielding covering the distance between mask and detector plane. An active Bismuth Germanate Oxide (BGO) scintillator Veto system shields the detector bottom as well as the sides of the detector, up to the bottom of ISGRI (see op *of* the tube walls).

2.2 The imaging system

2.2.1 Collimator

In order to maintain the low-energy response of IBIS when dithering (see the document *Mission Overview, Policies and Procedures*), the collimation baseline consists of a passive lateral shield that limits the solid angle (and therefore the cosmic γ-ray background) viewed directly by the IBIS detector in the full field of view up to a few hundred keV. The tube collimation system is implemented with three different devices:

Hopper: Four inclined walls starting from the detector unit with a direct interface to the IBIS detector mechanical structure. The inclination of the hopper walls should ideally be such that the area laid out by the bottom of walls matches the mask size, but the true inclination takes into account the presence of the Calibration System and the mechanical constraints. The hopper walls reach 550 mm out from the ISGRI top plane (850 mm from the PLM base) while the actual height is 530 mm. The shielding effect is obtained with Tungsten foils embedded in the four hopper walls. The hopper walls thickness is 1 mm. The hopper is not physically connected to the payload module structure.

Tube: The Tube is formed of four payload module walls, and shielded with glued lead (Pb) foil. Two of the tube walls (± Z axis) are inclined (by about 3.5° to the vertical) in order to follow as closely as possible the inclined tube shape, whilst the Y-axis walls are vertical. In particular the actual inclination of the Z walls is defined by the interface requirements with the hopper: the Z Tube walls stop at 20 mm in the horizontal plane from each upper edge of the hopper walls, i.e., at 850 mm from the base of the Payload Module (PLM).

Mask side shielding: Four strips of 1 mm thick Tungsten, provide shielding from the diffuse background in the gaps between the mask edges and the top of the tube walls

2.2.2 The mask assembly

The IBIS Mask Assembly is rectangular with external dimensions of 1180 × 1142 × 114 mm^3, and consists of three main subsystems: the Coded Mask, the Support Panel and the Peripheral Frame with the necessary interface provisions.

Coded Mask is a square of size 1064 × 1064 × 16 mm^3 made up of 95 × 95 individual square cells of size 11.2 × 11.2 mm^2. The cells form a Modified Uniformly Redundant Array (MURA) coded pattern of 53 × 53 elements (see *Figure 3*). Approximately half of the cells are opaque to photons in IBIS' operational energy range, offering 70% opacity at 1.5 MeV. The other half of the cells are "open", with an off-axis transparency of 60% at 20 keV.

Support Panel includes additional elements to support the mask, providing the necessary stiffness and strength to withstand the launch and the in-orbit operational temperatures.

Peripheral Frame reinforces the sandwich panel and provides the mechanical interfaces with the INTEGRAL PLM.

2.3 Detector assembly

The ISGRI and PICsIT detectors, both of which are situated "under" the coded mask, are separated by 9 cm. PICsIT is situated below ISGRI.

2.3.1 Upper detector layer: ISGRI

Cadmium Telluride (CdTe) is a II-VI semi-conductor operating at an ambient temperature; 0° ± 20° C is the optimum range. As CdTe detectors can be made to have a relatively small surface, they are ideally suited to build a pixellated imager with good spatial resolution. On the other hand, their small thickness (necessary to achieve good energy resolution) restricts their use to the low energy domain (50% efficiency at 150 keV). Providing spectral performances intermediate between those attained by the cooled Germanium spectrometers (SPI) and the scintillators (PICsIT), CdTe can be well used in the low energy domain (down to ~15 keV).

The CdTe layer is made of 8 identical Modular Detection Units (MDUs) each having 2048 pixels (see *Figure 3*) which are read out by 512 Application Specific Integrated Circuits, ASICs (4 channels per ASIC). Each MDU is connected independently to a Detector Bias Box (DBB) and to a Module Control Electronics (MCE) system which ensures the A/D conversion and provides other on-board processing such as event filtering and active pixel monitoring.

The specifications of the ISGRI layer are:

- Pixel (CdTe crystal) dimension: 4 x 4 mm^2, 2 mm thick
- Spacing between pixels: 600 μm (4.6 mm centre-to-centre)
- Minimum assembly: polycell of 16 pixels (4 x 4)
- MDU: 128 polycells (16 x 8)
- Layer: 8 MDUs (total of 8 x 64 x 32 pixels)
- Total sensitive area: 2621 cm^2 (16384 x 16 mm^2).

The CdTe layer is about 15 mm thick and is located at 294 mm above the PLM base plane.

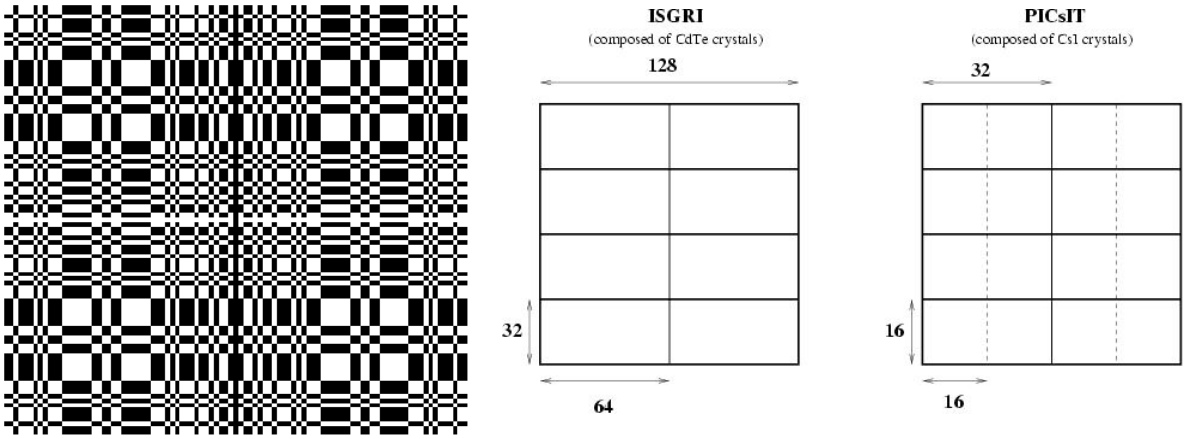

Figure 3. The IBIS coded mask model (left), and ISGRI and PICsIT detector module structure.

2.3.2 Lower detector layer: PICsIT

Caesium Iodide (CsI) is a I-VII scintillation crystal. The main characteristics of the layer are:

- Pixel (CsI) crystal dimension: 8.55 × 8.55 mm^2, 30 mm thick
- Spacing between pixels: 550 μm (9.2 mm centre-to-centre)
- Minimum assembly (ASIC): 16 pixels (4 × 4)
- Module: 32 ASICs
- Layer: 8 Modules (total of 8 × 32 × 16 pixels)
- Total sensitive area: 2994 cm^2 (4096 × 73.1 mm^2).

The CsI(Tl) bars are optically bonded to custom-made low-leakage silicon PIN photodiodes. The design provides a high degree of modularity. The CsI(Tl) layer is divided in 8 rectangular modules of 512 detector elements, each module being integrated into a stand-alone testable sub-system (see *Figure 3*). The CsI modules have the same cross-sectional shape as those of the CdTe.

2.4 Veto shield

The Veto shield is crucial to the operation of IBIS, because it is used as part of the anti-coincidence system to discriminate against background particles and photons propagating through or induced within the spacecraft.

The sides of the telescope up to the ISGRI bottom level and rear of the stack of detector planes, are surrounded by an active BGO Veto shield. Like the detector array, the Veto shield is modular in construction. There are 8 lateral shields, i.e., 2 modules per side, and 8 bottom modules. Each Veto Detector Module (VDM) includes:

- the BGO crystal and related housing
- two photomultiplier tubes (PMTs) optically coupled to the BGO and assembled with the dedicated Front End Amplifiers and High Voltage (HV) divider
- one HV Power Supply
- one Veto Module Electronics box for Module control
- internal harness.

The high density and mean Z of the BGO ensure that a thickness of 20 mm is sufficient to significantly reduce the detector background (caused by leakage through the shielding of cosmic diffuse and spacecraft-induced γ-rays), to less than the sum of all other background components.

2.5 Electronics

2.5.1 Analog Front End Electronics (AFEE)

Charge collection, signal filtering and amplification are all performed by the Application Specific Integrated Circuits (ASICs) on both ISGRI and PICsIT. In ISGRI, the 16384 individual detector units (pixels) are grouped into *polycells*. A polycell, the basic assembly unit of a detector module, is a hybrid circuit, which receives a signal from 16 detectors via 4 ASICs.

2.5.2 Module Control Electronics (MCE) and PICsIT Electronic Box (PEB)

The MCE and PEB perform receipt, checking and execution of telecommands for ISGRI and PICsIT, respectively. They also collect and format the housekeeping data and process the analogue and digital data (energy and rise time). An important function of the MCE is to monitor the CdTe noise levels. In-flight, a CdTe detector can become noisy and trigger the relevant MCE too frequently, causing a large dead time with unacceptable loss of photons. Therefore, the MCE monitors, in real time, the relative counting rates of each CdTe polycell. If a polycell exhibits noise, the MCE will, if necessary, switch it off (i.e., the pixel becomes "disabled" or "dead"). It can subsequently be reactivated and checked from the ground.

2.5.3 On-board calibration unit

IBIS contains an on-board collimated radioactive ^{22}Na source. This allows regular calibration of PICsIT at both the 511 keV and 1275 keV lines (calibration to better than about 1% in 1–2 orbits). ISGRI can also use the 511 keV line, albeit at lower efficiency.

2.5.4 Digital Front End Electronics (DFEE) and "FIFO"

The DFEE is situated behind the AFEE and processes the ASICs output for the 'first-in, first-out' (FIFO) data manager. FIFO sorts the events from different modules according to their true arrival time in the detector plane for transmission to the DPE/HEPI (see below). The DFEE also monitors the FIFO and instructs it when to send data to the DPE.

2.5.5 Data Processing Electronics (DPE) and Hardware Event Processor (HEPI)

The detector electronics chain ends at the DPE and the HEPI. The HEPI performs the data histogramming and generates the data structures for the DPE. The DPE handles all the interfaces between the instruments and the spacecraft for both uplink and downlink. For example, it handles the packetting of data for the On-Board Data-Handling System before transmission to the ground.

3 How the instrument works

3.1 Detection

Photons are detected in IBIS by several methods (Figure 4):

Detection in ISGRI: a photon is stopped in a single pixel of the semi-conductor, generating an electric pulse. Each photon that penetrates a CdTe pixel in ISGRI, ionizes the material and creates electron and hole pairs. In the polarizing electric field (bias voltage), the light and negatively charged electrons travel towards the positive electrodes faster than the heavier holes that move in the opposite direction. This movement of the charges (or current) induces a pulse whose height is directly proportional to the number of electron-hole pairs, and is subsequently amplified.

The detector coordinates, the pulse height and the rise time of each event are stored in the form of a list (raw data), from which, through the use of 2 look up tables, the deposited energy of an event can be reconstructed; the first one is used to transform the pulse height from a number of channels to an energy in keV and apply a gain correction, while the second combines the rise time and pulse height information to determine the charge loss correction that should be applied to recover the event energy. This ambiguity arises from the properties intrinsic to the CdTe crystal, which in certain cases leads to multiple values of energy for the same rise time (see Limousin et al. 2001, NIMPR A, 471, 174 for further details).

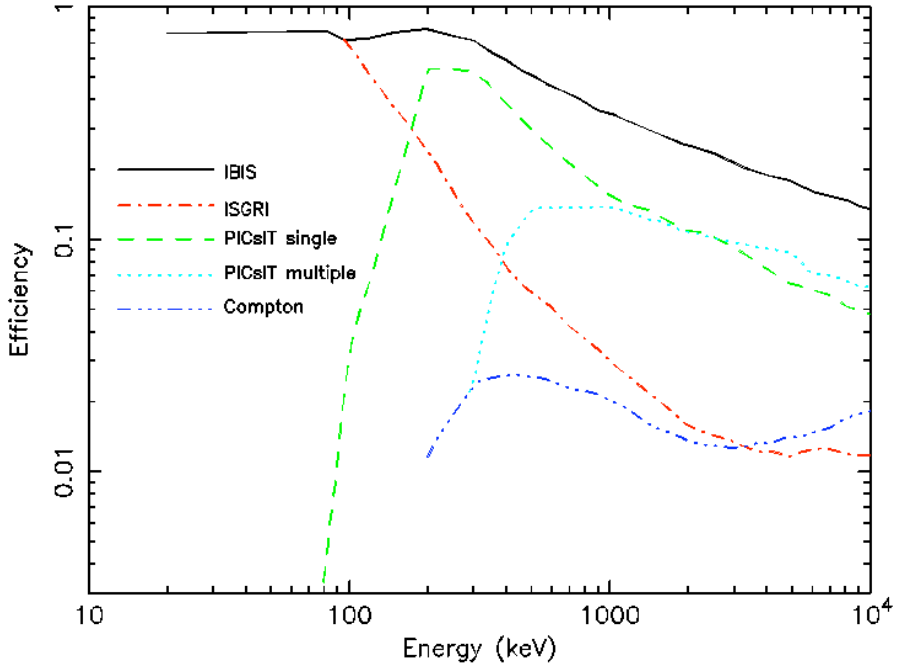

Figure 4. Detection efficiency evaluated by Monte Carlo simulation.

Detection in PICsIT: a photon passes through ISGRI and is stopped in PICsIT, generating one or more scintillation flashes. PICsIT records detections which occur in just one pixel (single events), and detections which occur in more than one pixel (multiple events), separately.

The energy of the incident photon is derived in each crystal bar from the intensity of the flash recorded in the photodiode. For multiple events, it is derived by summing the energies derived from the intensity of each of the flashes. The energy resolution of PICsIT is a function of the SNR of the events, the electronic noise at low energies and the light output.

Detection in both ISGRI and PICSIT (Compton mode): Photons arriving in either ISGRI or PICsIT may undergo a Compton scattering and be subsequently detected in the other layer. The energy of Compton events is determined from the sum of energies for the initial event and the photon scatter angle.

3.2 Imaging

IBIS has a field of view of 29°×29°. This means that a source contained within this field of view will cast a shadow of the mask onto the detector plane. However, given the geometry of the mask and hopper assembly, only sources within the central 8°×8 ° around the pointing direction will cast a complete shadow of the mask onto the detector. We therefore make the distinction between the Fully Coded Field Of View (FCFOV) and the Partially Coded Field Of View (PCFOV).

Since all sources present in the PCFOV contribute to the total detected flux, cross-correlation techniques are used to reconstruct the most probable configuration and intensity of the individual sources contributing to this flux.

The portion of the sky surveyed during an observation depends on the dither pattern. For the standard 5°×5° dither, the central 17°×17° are always fully coded, and a region spanning about 38°×38° is surveyed to zero response.

3.3 Timing

The ISGRI time resolution is 61.035 μs for each detected event. PICsIT spectra and images are accumulated every 1800-3600 seconds depending on the (flexible) dithering time; a spectrum alone (but with low resolution, from two to eight energy bands) is available every several ms.

3.4 Polarimetry

Multiple events in adjacent PICsIT cells can be used to determine the polarisation of the incident photons using the Klein-Nishina cross-section dependence on polarisation angle. Moreover, it is also possible to use the ISGRI and PICsIT detector planes in conjunction in order to select Compton events, allowing a reconstruction of the incident photon's polarisation (see Forot et al. 2008 for more details). Lists of Compton events per science window are now distributed with the data together with the ISGRI and PICSIT events.

3.5 Observing modes

IBIS has several observing modes for engineering and calibration purposes, but only one for scientific observations. In *science mode*, there are no user-selectable parameters, and ISGRI registers and transmits photon-by-photon: every event is tagged with its arrival time, energy, and position on the detector plane.

PICsIT can also operate in *photon-by-photon mode* (PPM), but because of its much higher background due to cosmic ray induced events, the limited telemetry does not allow operating in this mode because it would lead to important data losses. For this reason, the standard mode for PICsIT is *histogram mode*: registered events are integrated over the pointing duration (spectral imaging) or over the detector plane (spectral timing). It is, therefore, only possible to correct for the contribu- tion from cosmic-ray induced events a posteriori by statistical methods, whose statistical properties were evaluated using the PICsIT PPM data just after the instrument activation. At present the soft- ware removes consecutive events on a single pixel in PPM data, and resets pixel counts above a certain threshold to shadowgramme mean in spectral imaging histograms.

For the spectral timing data, both the time resolution that ranges between 0.976 and 500 ms, and the number of energy channels can be set from the ground. Currently, PICsIT uses a time resolution of 15.625 ms and 8 energy channels: 208–260, 260–312, 312–364, 364–468, 468–572, 572–780, 780–1196 and 1196–2600 keV. The characteristics of the different observing modes for IBIS are summarized in Table 2.

Table 2: ISGRI and PICsIT observing modes

	Observing Mode	Imaging resolution (pixels)	Timing resolution	Spectral resolution (channels)
ISGRI	photon-by-photon	128x128	61.035 μs	2048
PICsIT	photon-by-photon	64x64	64 μs	1024
	spectral-imaging	64x64	30-60 min	256
	spectral-timing	none	1-500 ms	2-8

4 Performance of the instrument

4.1 Components and sources of instrumental background

The bulk of the detected photons in both ISGRI and PICsIT are not from the scientific targets that are observed. These background photons are of two types: instrumental and astrophysical, and their main sources are:

- for ISGRI at low energies (< 100 keV): cosmic-ray induced fluorescence of the shielding elements, and diffuse cosmic γ-ray background.
- for ISGRI at higher energies and for PICsIT: radioactive decay of unstable nuclei created by the spallation interactions of cosmic-ray protons and their secondary particles in the massive parts of the satellite.

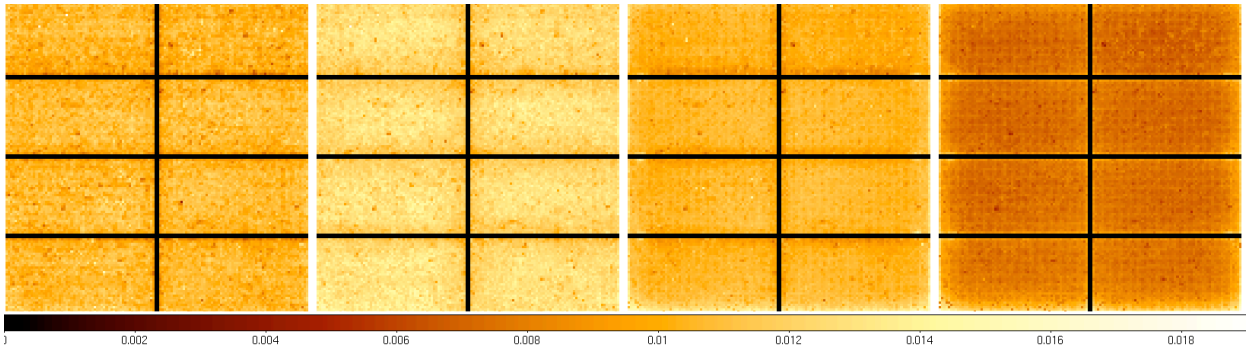

Figure 5. ISGRI time-averages intensity background maps in four logarithmically sized energy bands: 20-35, 35-60, 60-100 and 100-175 keV. The colourbar scale ranges from 0 to 0.018 cps, but the maps are re-normalized depending on the count rate in each science window.

The overall background is strongly influenced by solar activity: it is lowest at solar maximum, when a stronger solar magnetic field inhibits the propagation of cosmic rays into the inner solar system, and is about twice as high at solar minimum. Veto performance is another major influence on background levels. During the performance verification phase, it was found that the Veto can help to reduce the count rate by approximately 50% for ISGRI and 40% for PICsIT. Time-averaged, in-flight background spectra as observed by ISGRI and PICsIT are shown in Figure 7, and the in-flight background rates are compared to those of the Crab on-axis in Table 3.

Since the background is strongly energy-dependent below ~100 keV, background cubes (2D-images as a function of energy) are constructed from all available empty fields and high latitude observations for each ISGRI energy channel (~0.5 keV). These are used by default in OSA, both for imaging and spectral analysis: the high resolution maps are rebinned to match the specified energy bands. An example of these background maps is shown in FIGURE 5.

From the first instrument activation, bursts in the PICsIT count rate were observed (see Figure 6). In the time-integrated detector images, they are seen as tracks of bright pixels, indicating that these events are related to the interaction of cosmic rays with the detector. The contribution of these cosmic-ray induced triggers to the total PICsIT background is of the order of 10%, but they mainly affect the low-energy channels below ~300 keV (up to about 30% of the total

background). Since in the standard observing mode only histograms are downloaded, this introduces non-statistical fluctuations in the data, up to a factor of a ~2.5 in the SNR. A study to remove these fake events onboard is ongoing.

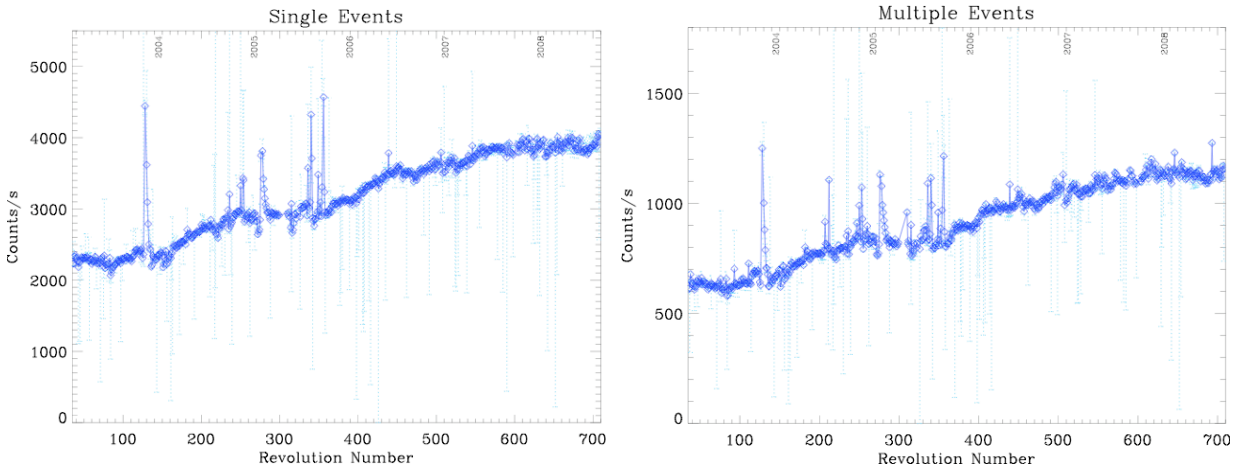

Figure 6: Total PICsIT count rate as a function of time (revolution number), computed with OSA 7 at the science window level, for single (left) and multiple events (right).

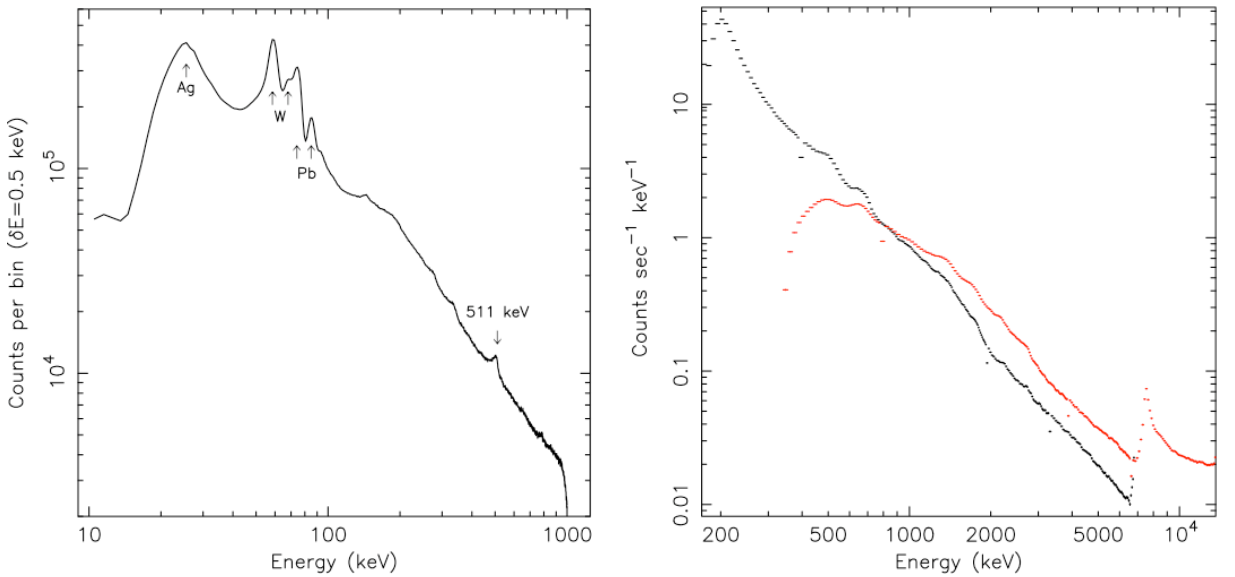

Figure 7. In-flight background spectra for ISGRI (left) and PICsIT (right) with OSA 7. The ISGRI spectrum is from empty field observations in revolution 96 (effective exposure time 36.4 ks). For PICsIT the single (black) and multiple (red) events contributions to the background are shown separately; based on one Science Window of data accumulated in revolution 500.

Table 3. Background rates compared to the Crab rates (OSA 6)

Energy band	Background (Solar Max) cts s^{-1}	Crab on-axis cts s^{-1}	
ISGRI: 15-400 keV	600	250	
PICsIT:		single	multiple
203-252 keV	–	2.71±0.02	–
252-336 keV	–	2.46±0.01	–
336-448 keV	–	1.17±0.01	0.07±0.01
448-672 keV	–	0.60±0.01	0.14±0.01
672-1036 keV	–	0.26±0.01	0.14±0.01
1036-1848 keV	–	0.06±0.01	0.12±0.01
(203-1036 keV; single)	2500	7.20±0.03	–
(336-1848 keV; multiple)	580	–	0.47±0.02

IBIS is located next to SPI and JEM-X, both also coded-mask telescopes. Since gamma-rays are highly penetrating, it is possible for them to pass through parts of the spacecraft or instrument structures, as well as coded masks, and to be detected by the gamma-ray instruments. Therefore, off-axis gamma-rays (effectively those with energies above ~300 keV) that pass through either the SPI or the JEM-X coded masks may cast a shadow of this mask onto the IBIS detectors (see Figure 8). The former combination is often referred to as the ''SPIBIS'' instrument. Although it effectively increases the field of view of IBIS, a bright gamma-ray source would thus add additional counts and modulation to the IBIS histogram, which considerably complicates the image reconstruction.

The SPIBIS effect has been calibrated before launch. ISOC avoids scheduling sources when either of the three brightest sources/regions, i.e., Crab, Cyg X-1 or the Galactic Center region, are visible by IBIS through the SPI mask. This ensures that the observation is uncontaminated by a possible SPIBIS effect.

4.2 Instrumental characterisation and calibration

The ISGRI and PICsIT detectors are calibrated in-orbit on a regular basis. Biannual observations of the Crab are performed to enable regular verification of the detector uniformity and energy response, and improve the calibration. Continued efforts to improve our understanding of the instruments and the mask assembly allow for a steady refinement of the analysis software. At present the calibration is good up to a level of a few percent for ISGRI, and about 5% for PICsIT at off-axis angles less than ~10°. This means that in the spectral fits the deviations between the observed spectrum and actual model are generally within 5% (see, for example, Figure 9).

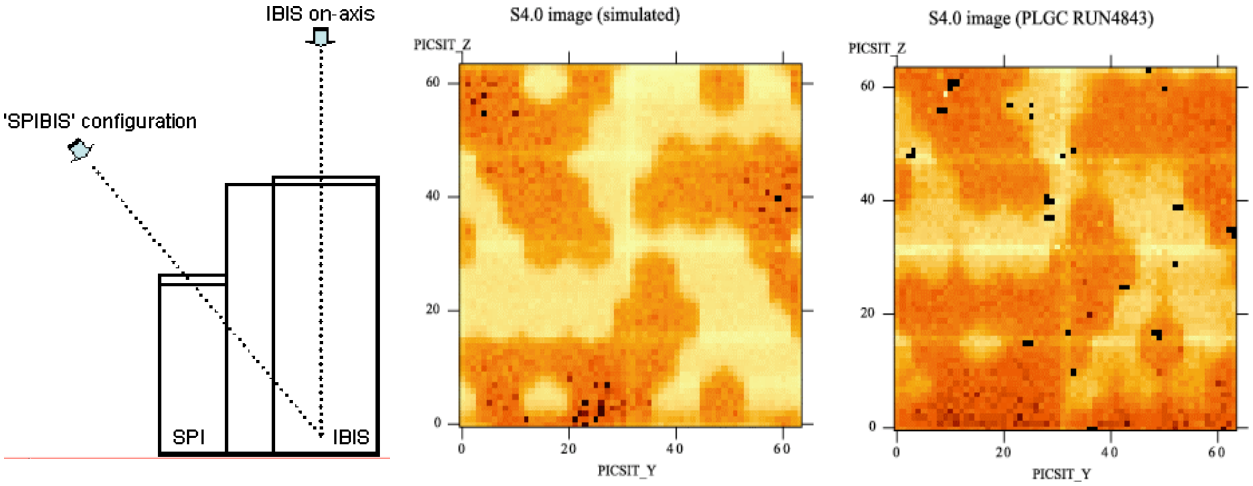

Figure 8: Left: Off-axis source positions for the SPIBIS configuration as well as the shielding tests, during the pre-flight calibrations. Middle and right: PICsIT shadowgrams from simulations (middle) and pre-flight calibration data (right). The images are slighhtly offset due to the inaccuracy in the supplied source position.

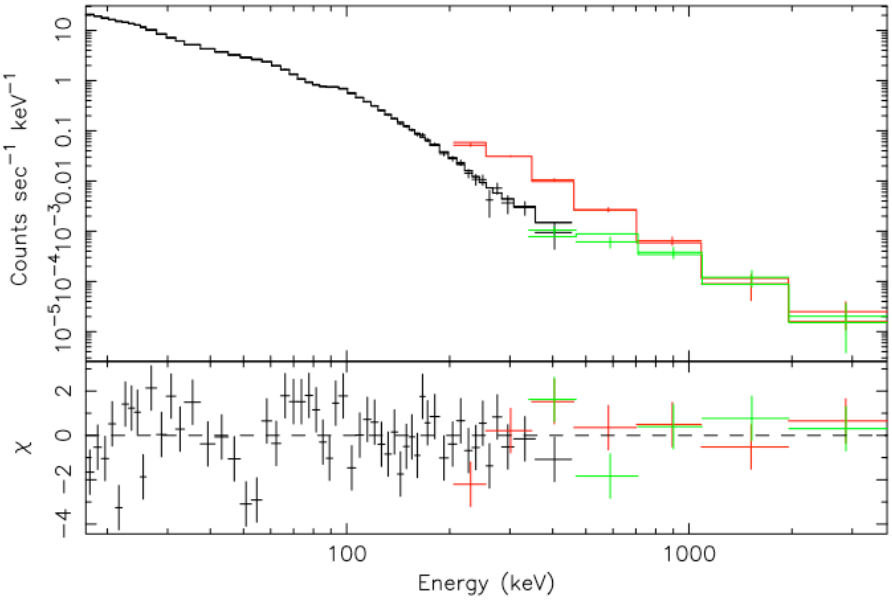

Figure 9. IBIS Crab photon spectrum. The fit to the data is done with a broken power-law model whose best fit parameters are $\Gamma_1 = 2.09^{+0.003}_{-0.015}$, $E_{break} = 96.27$ keV, and $\Gamma_2 = 2.29^{+0.056}_{-0.045}$, with a normalisation at 1 keV of 9.67 photons cm^{-2} s^{-1} keV^{-1}. The ISGRI data (black) was collected during an on-axis staring observation in revolutions 300 (net time of 31 ks), and the PICsIT data was collected in revolutions 39-45 (net time of 563 ks), for single (red) and multiple events (green). The analysis was done with OSA 7.0, and a systematic error of 1% was added to each spectral bin. The reduced is χ^2 =1.73 (χ^2 = 105.8 for 61 degrees of freedom). The intercalibration constant between ISGRI (set as reference) and PICsIT is 0.56±0.04.

The instrument characteristics are verified after events such as solar flares. The energy response and spectral resolution are monitored on long time-scales using the de-excitation lines at 511 keV and 1275 keV emitted by the on-board ^{22}Na calibration source, and at 59.3 keV using the background-induced Tungsten fluorescence line from the coded mask and hopper walls.

ISGRI shows a loss of gain of about 3% per year, and additional gain drops (0.6-1%) occurred after (strong) solar flares. Therefore, the data analysis software contains a time-dependent gain correction for ISGRI. Variations due to global temperature changes (~5°) are taken into account with an accuracy of 0.5%. Taking into account the expected PICsIT gain variation of 0.3% °C−1 measured during on-ground thermal tests, the average gain (over the whole detection plane) mea- sured in-flight indicates that the PICsIT temperature gradient along the INTEGRAL orbit is the dominant factor in the observed PICsIT gain variation. The current number of disabled pixels in ISGRI is stable at ~500 (of 16384 pixels) and ~52 (of 4096 pixels) in PICsIT.

At high energies (typically >1 MeV), the background so strongly dominates the flux of any cali- bration source that a large amount of data is needed. It was not possible to take sufficient measure- ments in the few weeks of the commissioning phase. Therefore, data accumulated through routine operations are used to extend the calibration into the MeV region.

4.3 Measured performance

4.3.1 Angular resolution and point source location accuracy

The angular resolution of IBIS is 12' FWHM. However, a feature of coded masks is that the centroiding accuracy for a point source can be much finer, depending solely on the detection significance (SNR). For ISGRI, the absolute localisation accuracy for sources detected with a significance of 100 in the FCFOV is as low as 20". With a detection significance of 10, the localisation radius increases to about 2'. For PICsIT, its PSLA is roughly a factor of two coarser (see Figure 10).

4.3.2 Spectral resolution

The spectral resolution of ISGRI has been measured during pre-flight tests on the engineering model, as well as in-flight (Figure 11). Resolutions of 9% at 60 keV (W fluorescence) and 4.6% at 511 keV have been measured from in-flight spectra. These results are in perfect agreement with the pre-flight measurements and show the stability of the instrument, even after disturbing events such as solar flares. Figure 11 shows the PICsIT spectral resolution, as determined in-flight. The in-flight data show no degradation or changes in the PICsIT spectral performance.

4.3.3 Off-axis response

The off-axis response of the IBIS telescope has been characterized during the Crab calibration observations in 2004, 2005 and 2006: the flux of off-axis sources could be underestimated by up to 50% in the PCFOV at low energies (around 20 keV). This loss is linked to the mask supporting structure (including the nomex structure), and strongly depends on the angle and the energy of the incoming radiation. The correction maps used in the imaging and spectral analysis software are shown in Figure 12; the residual off-axis effects after correction are less than a few percent.

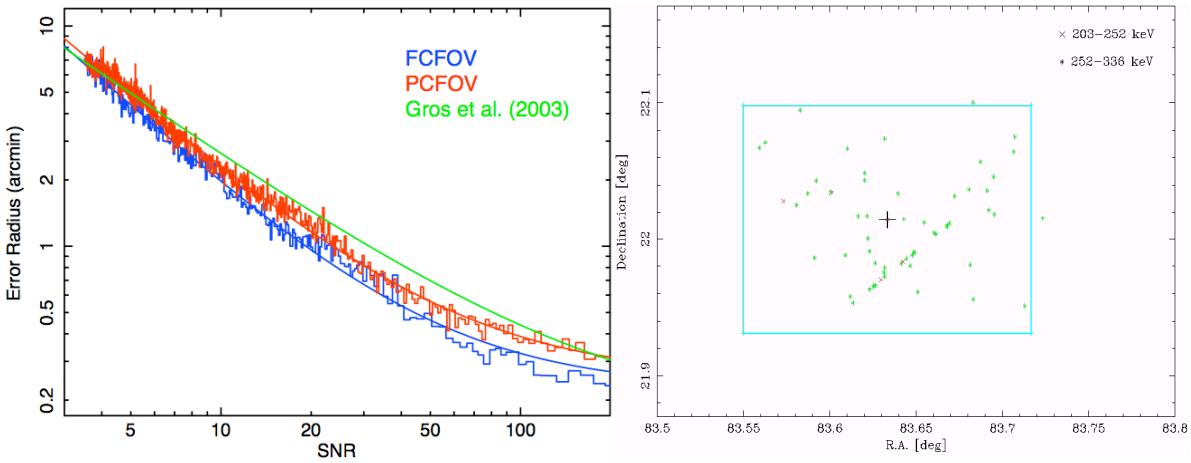

Figure 10: Left panel: ISGRI point source location accuracy (PSLA; 90% confidence level) in units of arcminutes for sources in the FCFOV using an analysis based on ~40000 science windows is given by: $31.1(SNR)^{-1.25} + 0.23$. (Scaringi et al. 2010, A&A, accepted). The resulting fits are shown for the FCFOV (blue) and the PCFOV (red), and are compared with the only previous determination of the PSLA by Gros et al. (2003, A&A 141, L179), that parametrized their fit as: $22.1(SNR)^{-0.95} + 0.16$. Right panel: PICsIT PSLA using Crab observations from revolutions 39, 43, 44 and 45. Results for 2 energy bands are given (203-252 keV and 252-336 keV). Only detections with at least 3σ in a science window (or exposure) are used. The catalog position of the Crab is maked by a cross, and the size of a PICsIT pixel (10') is indicated by the rectangle.

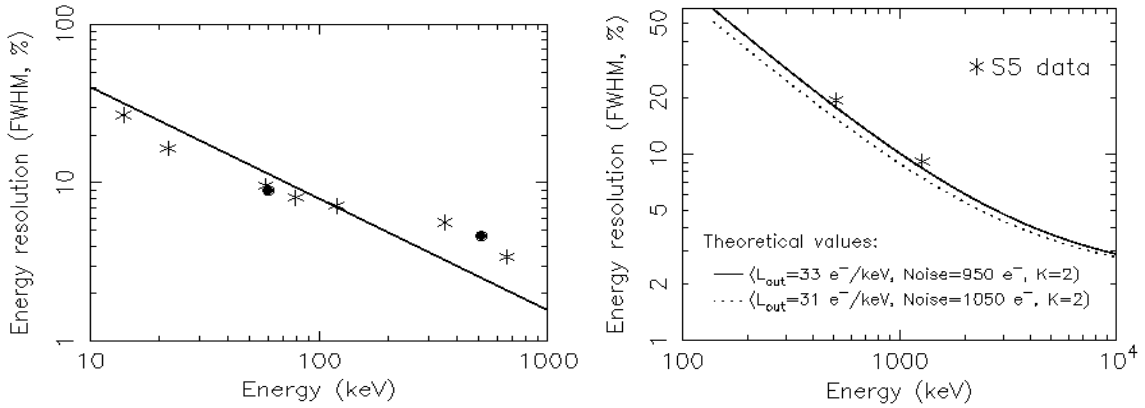

Figure 11. Left panel: The energy resolution of ISGRI. The solid line shows the theoretically expected values, and the stars are values measured before launch using an engineering model. The study of the in-flight W fluorescence line at 60 keV and the e^+/e^- annihilation lines at 511 keV (shown as filled circles) do not reveal any evidence of a change of the ISGRI spectral performance. Right panel: The energy resolution of PICsIT at 511 and 1275 keV as measured in-flight using Calibration Unit (S5) data (shown as stars). Also shown are the theoretical expectations as determined from pre-flight tests using an engineering model. The electronic-noise values ("Noise") refer to one ASIC only; a 10% increase is expected when extrapolating to the complete detector electronic chain.

Using the standard 5 × 5 dither pattern causes a slight (~2%) loss in overall sensitivity averaged over the dither pattern, but an important imaging advantage in smoothing out systematic effects. This mode is recommended for all observations except under special circumstances that should be well motivated and justified.

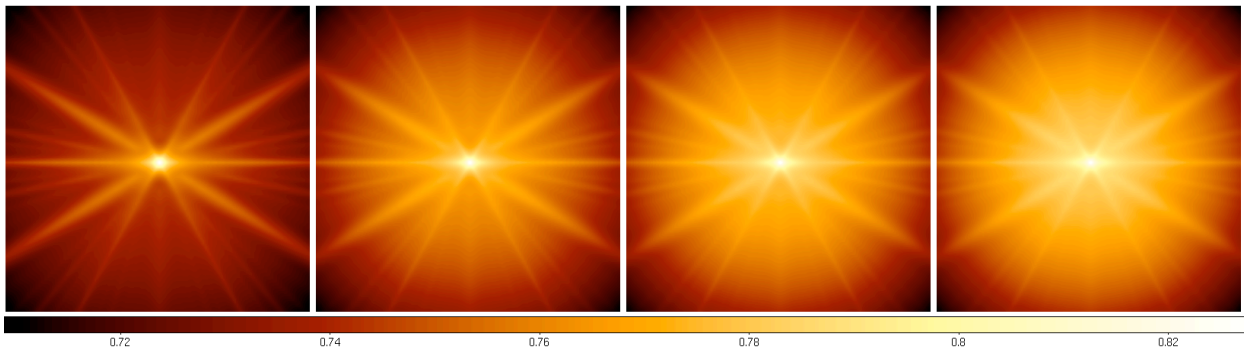

Figure 12: Off-axis correction maps based on a detailed nomex geometrical model in the energy bands 20-35, 35-60, 60-100 and 100-175 keV. In these new maps, there is an important non-axi-symmetric component characterized by the star-like shape, which is due to the hexagonal honeycomb structure of the nomex. Since these maps are used to correct the count rate, they are normalized to 1. In this example, the colourbar scale ranges from 0.71 to 0.83.

4.3.4 Sensitivity

The ISGRI and PICsIT broadband, statistically limited continuum and line sensitivity curves are parametrised as follows:

Continuum

$$S_c = \frac{n_\sigma^2\left(\vartheta_o + \vartheta_c\right)^2 + n_\sigma\left(\vartheta_o - \vartheta_c\right)\sqrt{2n_\sigma + 4T\Delta E \cdot A \cdot B}}{T \cdot \Delta E \cdot A \cdot \varepsilon_I \cdot \varepsilon_T\left(\vartheta_o - \vartheta_c\right)^2}$$

Line

$$S_L = \frac{n_\sigma^2\left(\vartheta_o + \vartheta_c\right)^2 + n_\sigma\left(\vartheta_o - \vartheta_c\right)\sqrt{2n_\sigma + 4T\Delta E \cdot A \cdot B}}{T \cdot A \cdot \varepsilon_P \cdot \left(\vartheta_o - \vartheta_c\right)^2}$$

where:

- S_c is the continuum sensitivity in photons cm^{-2} s^{-1} keV^{-1}
- S_l is the line sensitivity in photons cm^{-2} s^{-1}
- n_σ is the detection significance in units of sigma
- ϑ_o, ϑ_c are the open and closed mask element transparencies
- T is the observation duration
- ΔE is the energy bin (continuum),
- δE is the energy resolution,
- A is the detector area,
- B is the background count rate in counts cm^{-2} s^{-1} keV^{-1}
- ε_I is the imaging efficiency, a function of the coding noise and dither pattern

- ε_p, ε_T are the peak and total efficiencies,

Note that for a broad line with a FWHM of ΔE keV, the sensitivity is reduced by $(\Delta E/\delta E)^{1/2}$.

Figure 13 shows these sensitivities as derived from empty field observations and calculated using OSA 7. Tables 4, 5 and 6 give some of the actual values. Note that the PICsIT sensitivities have not changed with respect to AO-3 esitmates. They agree with the observed sensitivities within a factor of ~2. This difference is due to systematics, which increase partly due to long observations (typically >500 ks), and partly due to a large number of source in the range 20–150 keV. The latter does not affect the sensitivity at higher energies where there are few bright sources.

Table 4. ISGRI continuum sensitivities for an on-axis source

Energy band	Measured SNR (1)	Expected Crab flux (2) (ph cm^{-2} s^{-1})	Measured sensitivity (3) (ph cm^{-2} s^{-1})	Statistically limited sensitivity (AO5) (3) (ph cm^{-2} s^{-1})	Ratio (meas./AO5)
20-40 keV	1655	13.65×10^{-2}	13.45×10^{-6}	10.39×10^{-6}	1.3
40-100 keV	1006	7.36×10^{-2}	4.56×10^{-6}	5.02×10^{-6}	0.9
100-200 keV	272	2.22×10^{-2}	2.69×10^{-6}	3.12×10^{-6}	0.9

(1): Derived from Crab observations performed in Revolution 102 (see IBIS/ISGRI Validation Report V3.0, available at http://www.isdc.unige.ch/integral/download/osa_doc).
(2): Using a power-law with photon index of 2.12 and a flux at 1 keV of 8 ph cm^{-2} s^{-1} keV^{-1}.
(3): Sensitivities for an exposure of 100 ks, $\Delta E=E/2$, 3σ at 30, 70 and 150 keV.

Table 5. ISGRI continuum sensitivities
(10^5 s exposure, 3σ detection, $\Delta E=E/2$)

Energy (keV)	ph cm^{-2} s^{-1} keV^{-1}	Energy (keV)	ph cm^{-2} s^{-1} keV^{-1}	Energy (keV)	ph cm^{-2} s^{-1} keV^{-1}
15	12.8×10^{-6}	60	6.36×10^{-6}	300	6.02×10^{-6}
20	18.0×10^{-6}	70	5.02×10^{-6}	350	6.90×10^{-6}
25	16.0×10^{-6}	80	3.94×10^{-6}	400	7.56×10^{-6}
30	10.4×10^{-6}	90	3.46×10^{-6}	450	8.41×10^{-6}
35	7.54×10^{-6}	100	2.85×10^{-6}	500	9.83×10^{-6}
40	6.16×10^{-6}	150	3.12×10^{-6}	600	10.6×10^{-6}
45	5.59×10^{-6}	200	4.10×10^{-6}	700	11.6×10^{-6}
50	5.40×10^{-6}	250	5.03×10^{-6}	800	12.7×10^{-6}

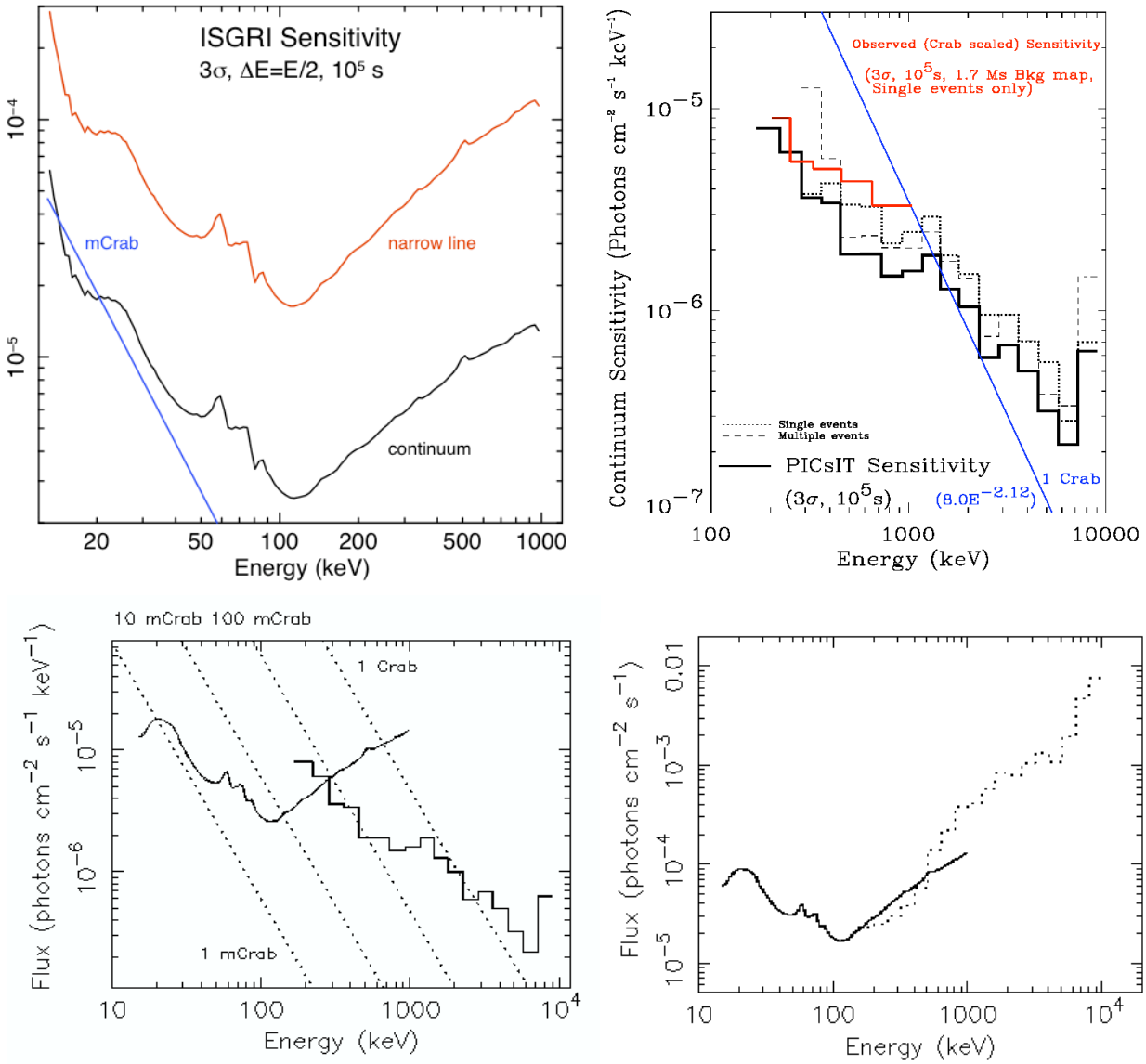

Figure 13: Top Left: ISGRI continuum (black: ph cm−2 s−1 keV−1) and narrow line sensitivity (red: ph cm−2 s−1) derived from 77 ks of empty field observations processed with OSA 7. Top Right: PICsIT statistically limited continuum sensitivity is given by the black histograms, from single events (dotted), multiple events (dashed), and combined (solid), all scaled to the in-flight background count rate, and compared with the sensitivity obtained by scaling from the Crab observation using OSA 5 (red; single events only). Bottom panels: IBIS broadband sensitivity derived from empty field observations for a 3σ detection in 105 s for a continuum source (ΔE = E/2; left) and a narrow line (right). Systematic uncertainties (e.g., uniformity) are not taken into account. ISGRI covers 15–1000 keV and PICsIT 200–104 keV (single and multiple). Reference fluxes are for a power-law Γ=-2.

Table 6. PICsIT continuum sensitivities (10^5 s, 3σ, ΔE=E/2; single and multiple events)

Start energy (keV)	End energy (keV)	ph cm^{-2} s^{-1} keV^{-1}	Start energy (keV)	End energy (keV)	ph cm^{-2} s^{-1} keV^{-1}
170	220	7.99×10^{-6}	1200	1400	1.88×10^{-6}
220	280	6.06×10^{-6}	1400	1800	1.28×10^{-6}
280	370	3.62×10^{-6}	1800	2200	1.05×10^{-6}
370	430	3.41×10^{-6}	2200	2900	0.59×10^{-6}
430	580	1.90×10^{-6}	2900	3500	0.68×10^{-6}
580	720	1.91×10^{-6}	3500	4500	0.50×10^{-6}
720	900	1.48×10^{-6}	4500	5700	0.32×10^{-6}
900	1200	1.57×10^{-6}	5700	7100	0.22×10^{-6}

Table 7. ISGRI and PICsIT narrow line sensitivity (10^6 s, 3σ detection)

Energy (keV)	ISGRI line ph $cm^{-2}s^{-1}$	PICsIT line ph $cm^{-2}s^{-1}$	Energy (keV)	ISGRI line ph $cm^{-2}s^{-1}$	PICsIT line ph $cm^{-2}s^{-1}$
22.5	8.76×10^{-5}		566.1	8.40×10^{-5}	14×10^{-5}
28.4	6.28×10^{-5}		712.6	9.88×10^{-5}	22×10^{-5}
35.7	3.92×10^{-5}		897.2	11.9×10^{-5}	38×10^{-5}
45.0	3.13×10^{-5}		1129.5		$41x\ 10^{-5}$
56.6	3.71×10^{-5}		1421.9		57×10^{-5}
71.3	3.08×10^{-5}		1790.1		82×10^{-5}
89.7	2.17×10^{-5}		2253.6		79×10^{-5}
112.9	1.67×10^{-5}		2837.1		100×10^{-5}
142.2	1.98×10^{-5}		3571.7		$130x\ 10^{-5}$
179.0	2.54×10^{-5}	2.3×10^{-5}	4496.5		110×10^{-5}
225.4	3.21×10^{-5}	2.5×10^{-5}	5660.7		200×10^{-5}
283.7	4.27×10^{-5}	3.0×10^{-5}	7126.5		470×10^{-5}
357.2	5.31×10^{-5}	3.8×10^{-5}	8971.6		760×10^{-5}
449.6	6.64×10^{-5}	5.7×10^{-5}			

4.3.5 Timing

The *time resolution* in ISGRI is 61.035 μs. For PICsIT, imaging and spectral histograms are collected every 1800-3600 seconds (depending on the flexible dithering time) - there is no finer time resolution available inside the histogram. The spectral timing data of PICsIT (no imaging!) will be accumulated every few ms; the resolution can be selected from ground and can take a value between 0.976 and 500 ms. The value used in routine operations is15.625 ms.

The *absolute timing accuracy,* i.e., the barycentric correction to event times measured in IBIS depends on the time resolution and on the time frame synchronisation in the instrument and spacecraft subsystems, and the uncertainty in the spacecraft position. Calculations give an accuracy of 61 μs within 1σ, and 92 μs within 3σ. In-flight measurements show that the relative timing between instruments is within 10 μs, whereas the absolute timing accuracy is about 40 μs. A more accurate calibration might be performed via dedicated millisecond pulsar observations.

A detailed analysis based on the pulse profile analysis of the accretion powered pulsar (245 Hz) IGR J17511-3057 comparing the absolute timing abilities of ISGRI and RXTE's HEXTE and PCA, shows that measurements with these three instruments are consistent with each other at the level of 50 μs (Lucien Kuiper, private communication).

We distinguish between the instrument's actual detection efficiency, and the delay or instrumental dead time that follows each detected event and during which another event can not be recorded. The BGO shielding, calibration source, and Compton coding induce additional dead times due to good events that happen to occur during their respective time windows.

In ISGRI dead time is around 25%, and is due to the combined effects of:

- Detected ISGRI events (115 μs each)
- VETO strobe length (ISGRI: 5 μs, PICsIT: 2 μs)
- Calibration source (negligible)
- Compton coincidence window for each PICsIT detection (3.8 μs per window; negligible)

PICsIT dead time is about 5%. For additional details, see the latest version of the IBIS Analysis User Manual at http://www.isdc.unige.ch/integral/download/osa_doc.

5 Observation "Cook book"

In this section, there are examples on how to calculate the observation time required to attain various scientific aims. For a panoramic view of the science that can be done with INTEGRAL, browse the INTEGRAL Image Gallery at
http://www.sciops.esa.int/index.php?project=INTEGRAL&page=Image_Gallery

5.1 How to calculate observing times

The approximate signal-to-noise ratio (SNR) for a given exposure can be calculated from the sensitivity curves. As shown in §4.3.4, the continuum sensitivity, S_{cont}, scales with SNR, $t^{-1/2}$, and $\Delta E^{-1/2}$; and the line sensitivity S_{line} as SNR and $t^{-1/2}$. Therefore, for an observation time, t in seconds, $\Delta E/E$, and continuum, F_{cont} in ph cm−2 s−1 keV−1, or line flux F_{line} in ph cm−2 s−1, we find:

$$\mathrm{SNR(cont)} = 3\left(F_{\mathrm{cont}}/\mathrm{S}_{\mathrm{cont}}\right)\left(2\Delta E/E\right)^{1/2}\left(t/10^{5}\right)^{1/2}$$

$$\mathrm{SNR(line)} = 3\left(F_{\mathrm{line}}/\mathrm{S}_{\mathrm{line}}\right)\left(t/10^{6}\right)^{1/2}$$

Recall that if the line is broader than the energy resolution of the instrument, with a FWHM of ΔE, then the signal-to-noise ratio is reduced by $(\Delta E/\delta E)^{1/2}$, where δE is the instrumental FWHM at that energy.

The above back-of-the-envelope calculation is indicative of what can be achieved. For proposals, observer should use the much more accurate on-line Observation Time Estimator (OTE) found on the ISOC web site http://integral.esa.int, as it is the means by which ISOC performs this type of calculation when assessing the technical feasibility of a proposed observation.

Continuum sensitivity values given in §4.3.4 are for monochromatic fluxes (ph cm^{-2} s^{-1} keV^{-1}), $\Delta E = E/2$, and can be reliably extrapolated to small energy ranges. However, when ΔE is greater than $E/2$, the energy range must be split into smaller energy bands each with ΔE smaller than $E/2$, in order to calculate the SNR or exposure times in each one, and then combine the results to get the values corresponding to the initial energy range. OTE does this using an input power-law spectral index.

5.2 Sample calculations

5.2.1 Example 1: hard transient at 100 keV

For a hard transient with a flux of 100 mCrab at 100 keV and a hard power law (photon spectral index Γ of -1) continuum above 100 keV, determine the achievable signal-to-noise ratio at 100 keV in an energy bin corresponding to the instrument FWHM at that energy.

Extrapolating the 2-10 keV flux of the Crab to the γ-ray band with a photon spectral index Γ=-2.1, he flux at 100 keV of a 100 mCrab source is: $F_{cont} = 6.9 \times 10^{-5}$ photons cm^{-2} s^{-1} keV^{-1}.

At this energy, only ISGRI can detect the source because it is below PICsIT's energy range. At 100 keV, ISGRI's energy resolution is $\Delta E/E = 0.08$ (see Figure 11), and its sensitivity is given by Figure 13 and Table 5 as:

$$S_{\text{cont}} = 2.85 \times 10^{-6} \text{ ph cm}^{-2}\text{s}^{-1} \text{ keV}^{-1}$$

If we assume an observation time of 50 ks, $t = 5 \times 10^4$ s, the equation above yields:

$$\text{SNR}_{\text{cont}} = 3 \times \left(6.9 \times 10^{-5}/2.85 \times 10^{-6}\right) \times \left(2 \times 0.08\right)^{-1/2} \times \left(5 \times 10^4/10^5\right)^{1/2} = 20.5$$

For these parameters and a 5×5 dither pattern, OTE gives a value of 20σ. Note that OTE also shows that the source is detectable with a significance of 10σ in 13 ks.

5.2.2 Example 2: hard transient at 800 keV

Consider the same source as in Example 1, but at 800 keV. Extrapolation of the 100 keV flux to 800 keV gives $F_{cont} = 8.5 \times 10^{-6}$ photons cm^{-2} s^{-1} keV^{-1}.

At 800 keV, PICsIT has the higher sensitivity. From Figure 13, Table 5 and Table 6, we find:

$$S_{\text{cont}} \text{ (ISGRI)} = 1.3 \times 10^{-5} \text{ ph cm}^{-2}\text{s}^{-1} \text{ keV}^{-1}$$

$$S_{\text{cont}} \text{ (PICsIT)} = 1.5 \times 10^{-6} \text{ ph cm}^{-2}\text{s}^{-1} \text{ keV}^{-1}$$

Since the sensitivity compared to source flux is lower at 800 keV than at 100 keV, we use a larger energy bin of $\Delta E/E = 0.15$. For the same 50 ks observation time we find:

$$\text{SNR}_{\text{cont}}\text{(ISGRI)} = 0.8 \quad \text{and} \quad \text{SNR}_{\text{cont}}\text{(PICsIT)} = 6.6$$

For this observation performed with a 5×5 dither, OTE gives 0.8σ and 6.4σ respectively. The source would, therefore, be detected by PICsIT but not by ISGRI. OTE also shows that to detect the source to 10σ, PICsIT needs an exposure time of ~123 ks, whereas ISGRI would require about 8.6 Ms.

5.2.3 Example 3: hard transient in broad band

Consider a transient with the same characteristics as the one seen in the previous examples, but for which only the broadband 50–150keV flux is known to be $F_{cont} = 7.6 \times 10^{-5}$ photons cm^{-2} s^{-1} keV^{-1}. For a 50 ks observation, taking a power-law spectrum with $\Gamma = -1$.

I n this case, OTE splits the 50-150 keV band into three narrower bands: 50–83 keV, 83–138 keV and 138–150 keV. Table 8 shows the OTE flux, ISGRI sensitivity, and SNR calculated using both Equation 4 (in column 4) and OTE for a 5 × 5 dither (in column 5). Combining in quadrature the SNR values in column 4 to get the 50–150 keV detection significance, we find $\text{SNR}_{\text{cont}} = 70$, compared to $\text{SNR}_{\text{cont}} = 61$ using the OTE values in column 5, and to $\text{SNR}_{\text{cont}} = 80$ if we use the equation in §5.1 (p. 27).

$$\text{SNR}_{\text{cont}} = 3 \times \left(7.6 \times 10^{-5}/2.85 \times 10^{-6}\right) \times \left(2 \times 100/100\right)^{-1/2} \times \left(5 \times 10^4/10^5\right)^{1/2} = 80$$

Table 8. OTE example calculation of detection significance in a broad band

Energy band (keV)	Flux (ph cm^{-2} s^{-1} keV^{-1})	Sensitivity (ph cm^{-2} s^{-1} keV^{-1})	SNR	SNR (OTE; 5×5 dither)
50-83	1.06×10^{-4}	5.0×10^{-6}	45	40
83-138	0.64×10^{-4}	2.6×10^{-6}	52	44
138-150	0.48×10^{-4}	3.0×10^{-6}	14	13

5.2.4 Example 4: ^{22}Na line at 1.275 MeV

We are searching for the ^{22}Na line at 1.275 MeV (half life of 3.5 yr) in a bursting transient source. The model-predicted line flux after outburst is: $F_{line} = 10^{-3}$ ph cm^{-2} s^{-1}. The PICsIT line sensitivity given in Figure 13 and Table 7 is: $S_{line} = 4.8 \times 10^{-4}$ ph cm^{-2} s^{-1}.

For a 500 ks observation, the equation in §5.1 (p. 27) predicts a detection significance of:

$$SNR_{cont} = 3 \times \left(10^{-3}/4.8 \times 10^{-4}\right) \times \left(5 \times 10^{5}/10^{6}\right)^{1/2} = 4.4$$

Similarly, OTE predicts an $SNR_{line} = 4.1$ for such an observation using the 5×5 dither. Moreover, OTE indicates that increasing the detection significance to a value of 10 would require an exposure time of ~3 Ms.